partment for formation of secondary lymphoid organs.

Our findings illustrate a novel function for IKKα that depends on its protein kinase activity and cannot be compensated by the related IKKβ subunit. Although both IKK catalytic subunits are involved in the activation of NF-κB transcription factors, they do so via different mechanisms and substrates. IKKβ is the canonical activator of NF-κB in response to infection and inflammation, and IKKα is responsible for activation of a specific NF-κB factor required for B cell maturation and formation of secondary lymphoid organs. This function is exerted through processing of NF-κB2 and is remarkably similar to the function of the *Drosophila* IKK complex, which contains a single catalytic subunit that is similar to both IKKα and IKKβ (*22, 23*). The DmIKK/Ird5 protein does not phosphorylate the single IκB of *Drosophila*, Cactus, and instead leads to activation of antibacterial genes through phosphorylation-induced processing of the *Drosophila* NF-κB1/2 homolog, Relish (*22, 23*). Although in *Drosophila* the processing-dependent NF-κB pathway is the major provider of innate antibacterial immunity (*23*), in mammals this pathway has been assigned to a specific aspect of adaptive immunity: B cell maturation and formation of secondary lymphoid organs. Thus, the duplication of IKK catalytic subunits and their functional divergence correlates with the evolution of the immune system.

References and Notes

1. S. Ghosh, M. J. May, E. B. Kopp, *Annu. Rev. Immunol.* **16**, 225 (1998).
2. D. M. Rothwarf, M. Karin, *Science's STKE,* stke.sciencemag.org/cgi/content/full/OC_sigtrans;1999/5/re1 (26 October 1999).
3. N. R. Rice, M. L. Mackichan, A. Israel, *Cell* **78**, 773 (1992).
4. F. Mercurio, J. DiDonato, C. Rosette, M. Karin, *Genes Dev.* **7**, 705 (1993).
5. M. Karin, Y. Ben-Neriah, *Annu. Rev. Immunol.* **18**, 621 (2000).
6. L. Lin, G. N. DeMartino, W. C. Greene, *Cell* **92**, 819 (1998).
7. H. C. Liou, W. C. Sha, M. L. Scott, D. Baltimore, *Mol. Cell. Biol.* **14**, 5349 (1994).
8. T. Yamada *et al.*, *J. Immunol.* **165**, 804 (2000).
9. R. Shinkura *et al.*, *Nature Genet.* **22**, 74 (1999).
10. L. Yin *et al.*, *Science* **291**, 2162 (2001).
11. G. Xiao, E. W. Harhaj, S. C. Sun, *Mol. Cell* **7**, 401 (2001).
12. N. L. Malinin, M. P. Boldin, A. V. Kovalenko, D. Wallach, *Nature* **385**, 540 (1997).
13. L. Ling, Z. Cao, D. V. Goeddel, *Proc. Natl. Acad. Sci. U.S.A.* **95**, 2791 (1998).
14. E. Zandi, Y. Chen, M. Karin, *Science* **281**, 1360 (1998).
15. Q. Li, D. Van Antwerp, F. Mercurio, K.-F. Lee, I. M. Verma, *Science* **284**, 321 (1999).
16. Z.-W. Li *et al.*, *J. Exp. Med.* **189**, 1839 (1999).
17. W. M. Chu *et al.*, *Immunity* **11**, 721 (1999).
18. U. Senftleben, Z.-W. Li, V. Baud, M. Karin, *Immunity* **14**, 217 (2001).
19. Y. Hu *et al.*, *Science* **284**, 316 (1999).
20. K. Takeda *et al.*, *Science* **284**, 313 (1999).
21. Y. Hu *et al.*, *Nature* **410**, 710 (2001).
22. N. Silverman *et al.*, *Genes Dev.* **14**, 2461 (2000).
23. Y. Lu, L. P. Wu, K. V. Anderson, *Genes Dev.* **15**, 104 (2001).
24. Fetal livers were harvested from embryonic day 16 wild-type, *Ikkα*$^{-/-}$, or *Ikkα*^{AA} embryos as described (*18*). Genomic DNA was genotyped using IKKα-specific primers (*19*). Single-cell suspensions were injected into the tail vein of lethally irradiated 8-week-old C57BL/6-CD45.1 female hosts (*18*). Mice were analyzed after 6 weeks or more. The donor origin of the analyzed cells was verified by CD45.2 staining (*18*).
25. See supplementary information at *Science* Online (www.sciencemag.org/cgi/content/full/293/5534/1495/DC1).
26. BrdU (Sigma) was administered for 7 days in the drinking water. DNA-incorporated BrdU was detected by flow cytometry after staining fixed (0.5% paraformaldehyde for 20 min) and permeabilized (3 N HCl and 0.5% Tween-20 followed by neutralization with 0.1 M disodium tetraborate) cells with a fluorescein-5-isothiocyanate–labeled antibody (BU-1, Becton Dickinson) in the presence of 0.5% Tween-20. B cells were marked by prestaining with anti-IgM (phycoerythrin-labeled R6-60.2, Pharmingen) and anti-IgD (11-26c.2a, Pharmingen) + anti-rat IgG [F(ab′)2, TC, Caltag]. Bone marrow cells from untreated and BrdU-treated mice served as negative and positive controls, respectively.
27. Lymphoid organs were fixed in 10% buffered formalin and embedded in paraffin. Sections were stained with hematoxylin and eosin for histological analysis. TUNEL (terminal deoxynucleotidyl transferase–mediated deoxyuridine triphosphate nick-end labeling) staining was performed using the In Situ Cell Detection kit (Boehringer Mannheim). For analysis of GC formation, mice were injected intraperitoneally (ip) with 100 mg of DNP-KLH absorbed to alum (Calbiochem) and spleens were collected 14 days later. Cryosections were stained with biotinylated PNA (Vector Laboratories), incubated with streptavidin peroxidase (Jackson Immunoresearch) for 30 min, and developed with 3,3′-diaminobenzidine (DAB) kit (Leinco Technologies). Sections were counterstained with hematoxylin (Sigma). For visualization of Peyer's patches, intestines were fixed in 0.5% paraformaldehyde, rinsed, and dehydrated in a methanol series. Endogenous peroxidase was inactivated with H_2O_2. After rehydration and blocking, the tissue was stained with anti-VCAM1 (Pharmingen) followed by staining with a secondary goat antibody to rat IgG conjugated to horseradish peroxidase. After washing, the tissue was developed with DAB kit.
28. A targeting vector in which the codons for Ser^{176} and Ser^{180} in the activation loop of IKKα were replaced by alanine codons was used to construct the *Ikkα*^{AA} allele. Full description and characterization of this mutant will be provided elsewhere (*34*). *Ikkα*^{AA} mice are viable, fertile, and morphologically indistinguishable from wild-type mice.
29. U. E. Gibson, C. A. Heid, P. M. Williams, *Genome Res.* **6**, 995 (1996).
30. T. Kaisho *et al.*, *J. Exp. Med.* **193**, 417 (2001).
31. G. Franzoso *et al.*, *J. Exp. Med.* **187**, 147 (1998).
32. H. Ishikawa, D. Carrasco, E. Claudio, R. P. Ryseck, R. Bravo, *J. Exp. Med.* **186**, 999 (1997).
33. A. Futterer, K. Mink, A. Luz, M. H. Kosco-Vilbois, K. Pfeffer, *Immunity* **9**, 59 (1998).
34. Y. Cao *et al.*, in preparation.

35. We thank C. Surh for advice on radiation chimeras, R. Rickert for many helpful and critical discussions, M. Delhase and V. Baud for advice and assistance with IKK and NF-κB assays, M. Matsumoto for advice on detection of Peyer's patches, C. Adams for manuscript preparation, and G. Ghosh and E. Raz for comments. Supported by postdoctoral fellowships from the Deutsche Forschungsgemeinschaft (U.S., F.R.G.), California Breast Cancer Research Project (Y.C.), Human Frontier Science Program (G.B.), Arthritis Foundation (Y.H.), NIH (grants AI434477 and ESO4151 to M.K. and AI45045 to S.-C.S.), and the California Cancer Research Program. M.K. is an American Cancer Society Research Professor.

18 May 2001; accepted 3 July 2001

Crystal Structure of Sensory Rhodopsin II at 2.4 Angstroms: Insights into Color Tuning and Transducer Interaction

Hartmut Luecke,[1,2]* Brigitte Schobert,[2] Janos K. Lanyi,[2]* Elena N. Spudich,[3] John L. Spudich[3]*

We report an atomic-resolution structure for a sensory member of the microbial rhodopsin family, the phototaxis receptor sensory rhodopsin II (NpSRII), which mediates blue-light avoidance by the haloarchaeon *Natronobacterium pharaonis*. The 2.4 angstrom structure reveals features responsible for the 70- to 80-nanometer blue shift of its absorption maximum relative to those of haloarchaeal transport rhodopsins, as well as structural differences due to its sensory, as opposed to transport, function. Multiple factors appear to account for the spectral tuning difference with respect to bacteriorhodopsin: (i) repositioning of the guanidinium group of arginine 72, a residue that interacts with the counterion to the retinylidene protonated Schiff base; (ii) rearrangement of the protein near the retinal ring; and (iii) changes in tilt and slant of the retinal polyene chain. Inspection of the surface topography reveals an exposed polar residue, tyrosine 199, not present in bacteriorhodopsin, in the middle of the membrane bilayer. We propose that this residue interacts with the adjacent helices of the cognate NpSRII transducer NpHtrII.

Microbial rhodopsins are a family of membrane-embedded photoactive retinylidene proteins found throughout the three domains of life: archaea (*1–3*), eubacteria (*4*), and unicellular eukaryotes (*5*, *6*). They share a common design of seven transmembrane helices forming an interior pocket for the chromophore retinal, and their functions are driv-

en by a common photochemical reaction—light-induced retinal isomerization—but they carry out two distinctly different functions: light-driven ion transport and photosensory signaling. Both functional types are found in haloarchaea such as *Halobacterium salinarum* and *Natronobacterium pharaonis*. In the haloarchaea, bacteriorhodopsin (BR) and halorhodopsin (HR) are light-driven ion pumps for protons and chloride, respectively (*2*, *3*); and the sensory rhodopsins I and II (SRI and SRII) are phototaxis receptors controlling the cell's swimming behavior in response to changes in light intensity and color (*1*). The *N. pharaonis* phototaxis receptor NpSRII is 27% identical to BR in amino acid sequence (*7*) and exhibits typically ~40% identity with other sensory rhodopsins; all contain ~80% identity in the residues known to form the retinal binding pocket in BR.

Atomic-resolution crystal structures of BR and HR from *H. salinarum* have been obtained by x-ray crystallography (*8*–*10*). An intermediate resolution (6.9 Å) projection structure of NpSRII derived from electron crystallography of two-dimensional (2D) crystals showed an overall disposition of the seven helices that was similar to that in the two transport rhodopsins (*11*). Here we report atomic-resolution information for a microbial sensory rhodopsin, the 2.4 Å structure of NpSRII obtained from x-ray diffraction of 3D crystals grown in a cubic lipid phase.

The overall seven-helical structure is similar to those of the transport rhodopsins BR and HR (*8*–*11*). The antiparallel β sheet at the BC loop is two residues shorter than in BR (*9*). The EF loop participates in crystal packing between bilayer sheets, and helix E is fully ordered with a π-bulge kink (*10*) at position 154. For data collection and refinement statistics, see Table 1.

Among the known photosensory pigments, a unique property of retinylidene proteins, in microbial rhodopsins as well as higher animal visual pigments, is the tuning of the absorption spectrum of the retinal chromophore over a wide range of the visible region. BR, HR, and SRI in *H. salinarum* absorb green-orange light, with absorption maxima at 570 to 590 nm, whereas SRII exhibits blue-shifted absorption maxima, at 487 and 497 nm for the *H. salinarum* and *N. pharaonis* homologs [HsSRII (*12*) and NpSRII (*13*, *14*)], respectively. A protonated retinylidene Schiff base compound in methanol/Cl^- exhibits maximal absorption at 440 nm (*12*). Interactions between the retinal chromophore and its protein environment typically shift the absorption to longer wavelengths (the "opsin shift") (*15*), resulting in absorption maxima at 497 nm in NpSRII and 568 nm in BR. In the better understood case, BR, three contributing factors have been identified (*16*): (i) the protein forces the con-

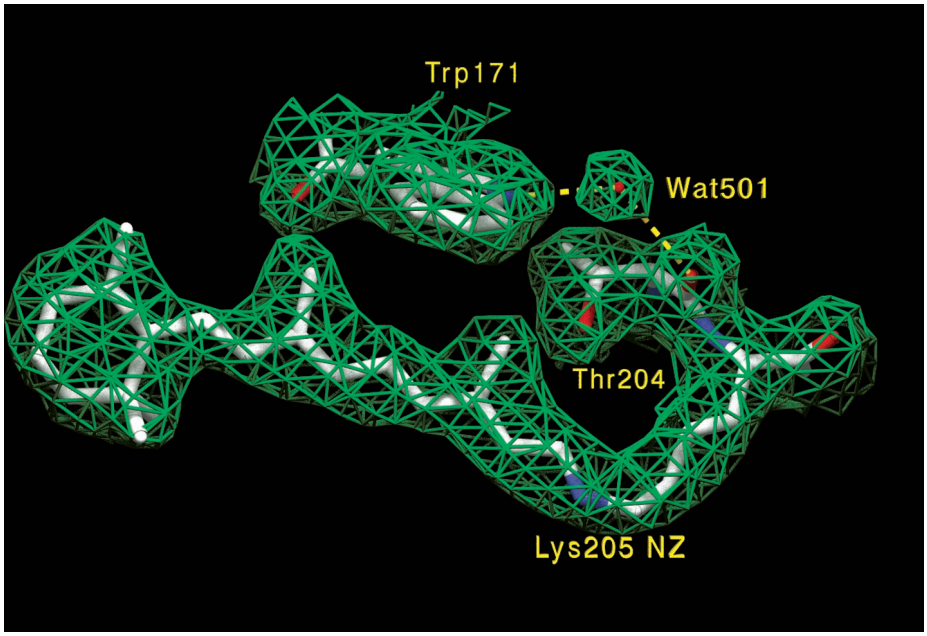

Fig. 1. Electron density map ($2|F_o| - |F_c|$, contoured at 1σ) and corresponding molecular model of the retinal binding pocket. As in BR and HR, the all-trans retinal polyene chain is coplanar with the beta-ionone ring, which is in the 6s-trans conformation. Wat^{501} is bridging helices F (Trp^{171}) and G (Thr^{204} carbonyl). In addition, Wat^{501} is also hydrogen-bonding with Thr^{167} OH (not shown).

Table 1. X-ray data collection, molecular replacement, and refinement statistics. Crystals were grown from a cubic lipid phase (*27*) using octylglucoside-purified NpSRII (28.0 mg/ml) preincubated with *H. salinarum* polar lipids (11.2 mg/ml) (*11*). Ten-microliter aliquots were mixed with 10 μl of monoolein glyceride (Nu-Check Prep., MI) and centrifuged for 1 hour at 11,000*g* at 22°C. After overnight incubation at 22°C, precipitant was added. The crystals used were thin rods about 5 μm by 20 μm by 200 μm and were examined 5 weeks after the addition of 50 μl of 3.5 M KCl in 50 mM MES (pH 5.3) as precipitant. Addition of exogenous *H. salinarum* polar lipids was essential for crystal formation. The crystals belong to space group $C222_1$, with $a = 87.34$ Å, $b = 130.81$ Å, and $c = 50.87$ Å, and consist of bilayers stacked in the *b* direction. The *a* and *c* cell dimensions, as well as the packing, are very similar to those reported for 2D crystals of NpSRII (*11*). Diffraction data were collected on one cryocooled crystal at the microfocus beamline ID13 at ESRF (Grenoble), using a MAR Research charge-coupled device detector. Each image was 1° in φ, with an exposure time of 2 s. Images were reduced, scaled, and merged with the programs DENZO/SCALEPACK (*28*). Molecular replacement was carried out with the program X-PLOR (*29*), using the coordinates of the 1.55 Å bacteriorhodopsin structure (PDB code 1C3W, protein without retinal) and yielded an initial *R* factor of 49.2% (4 to 12 Å). Successive rounds of refinement and model building with the programs CNS (*30*) and CHAIN (*31*) using annealed simulated omit and $3|F_o| - 2|F_c|$ maps resulted in an *R* factor of 23.3%, and an R_{free} of 28.0% for all data between 2.4 and 20 Å without σ cutoff. In many regions near the hydrophobic protein surface, long tubes of density are present for native dihydrophytyl lipids, which as in the case of BR remained tightly bound to the protein through solubilization and cubic lipid phase crystallization. All peptide bonds fall into the allowed regions of the Ramachandran plot.

Data reduction resolution range	*2.4–20.0 Å*	*2.40–2.44 Å*
Total observations	80,761	
Unique structure factors	10,704	520
R_{merge} (%)	9.5	44.0
Average $I/\sigma(I)$	5.7	1.3
Completeness (%)	92.2	92.0
Mosaicity (°)	0.86	
Refinement resolution range	*2.4–20.0 Å*	
R factor (%) for working set, no σ cutoff	23.3	
R_{free} (%) for 8.7% of the unique structure factors	28.0	
Deviation from ideal bond lengths (Å)	0.0086	
Deviation from ideal bond angles (°)	1.29	

[1]Department of Molecular Biology and Biochemistry, University of California, Irvine, CA 92697, USA. [2]Department of Physiology and Biophysics, University of California, Irvine, CA 92697, USA. [3]Department of Microbiology and Molecular Genetics and Structural Biology Center, University of Texas Medical School, Houston, TX 77030, USA.

*To whom correspondence should be addressed. E-mail: hudel@uci.edu (H.L.), jlanyi@orion.oac.uci.edu (J.K.L.), or john.l.spudich@uth.tmc.edu (J.L.S.).

formation of the C6–C7 single bond in the retinal to be 6s-trans, allowing ring/chain coplanarity; (ii) the positive charge on the protonated Schiff base is only weakly stabilized by a complex counterion provided by the protein environment; and (iii) a less well-defined third factor, which is thought to involve the interaction of polar or polarizable protein groups with the chromophore, destabilizes the ground state or stabilizes the excited state.

The retinal-binding pocket of NpSRII provides insights into structural changes responsible for its blue shift with respect to BR (Figs. 1 and 2). The ring and polyene chain of NpSRII are coplanar as in BR, and therefore we expect a similar opsin shift contribution from this factor. In the case of HsSRII, it has been suggested that ring/chain coplanarity alone is sufficient to explain its relatively small opsin shift to 487 nm (*12*).

Although one of the important means of modulating the absorption of a protonated retinal Schiff base is to vary its distance to its counterion (*15*), the two aspartate carboxyls Asp^{75} and Asp^{201} in NpSRII are in nearly identical positions as in BR. Instead, several changes in the structure combine to cause the blue shift from BR by minimizing factors (ii) and (iii), which shift BR absorption to longer wavelengths. The first is a displacement of the guanidinium group of Arg^{72} by 1.1 Å, coupled with a rotation away from the Schiff base in NpSRII. This increase in distance reduces the influence of Arg^{72} on the counterion, thus strengthening the Schiff base/counterion interaction.

Second, a blue shift is expected (*15*, *17*) from the removal of two hydroxyls near the β-ionone ring from Ser^{141} and Thr^{142} in BR, replaced with nonpolar residues Gly^{130} and Ala^{131} in NpSRII. A possible third contributor to the color difference is the change in tilt and slant of the retinal polyene chain, altering the interaction of the conjugated π system with the binding pocket, thereby modulating ground- and excited-state energy levels (Fig. 2A).

Mutagenic substitution of 10 residues, in or near the retinal-binding pocket with their corresponding BR residues, including Gly^{130} to Ser^{141} and Ala^{131} to Thr^{142}, produced only a ~25-nm red shift of the NpSRII absorption maximum (*18*, *19*). Our interpretation is that these substitutions do not produce the full 71-nm red shift to the BR value, because they do not result in the movements of Arg^{72} and

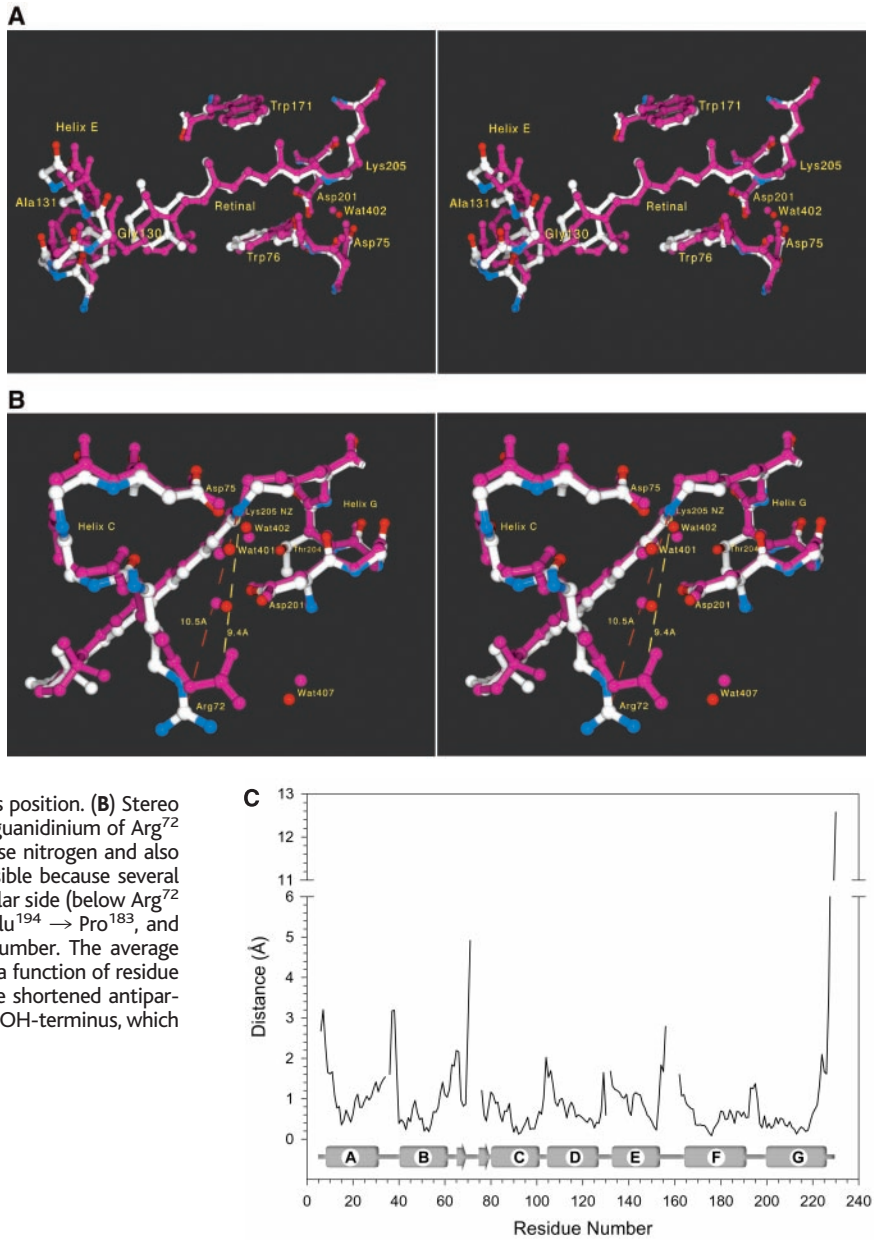

Fig. 2. Comparison of NpSRII and BR structures. The coordinates were aligned with the Iterative Magic Fit procedure of Swiss-PDBViewer version 3.7b2 (*33*), yielding a root mean square deviation of 0.96 Å for 816 main-chain atoms (BR is shown in purple; NpSRII is shown in white, blue, and red). (**A**) Stereo view of the retinal binding pocket. There is a change in the tilt of the whole polyene chain, presumably largely due to extra room near the end of the ring (C3 and C4 atoms) because of a combination of smaller side chains on residues 130/131 (Gly^{130}/Ala^{131} in NpSRII, Ser^{141}/Thr^{142} in BR) and a local outward bowing of the backbone of helices E and F by up to 1.3 Å [see (C)]. The Ser^{141}/Thr^{142} pair in BR, not labeled in the figure, contributes two hydroxyl groups, which are evident as purple protruding from helix E toward the ring. And despite equivalent retinal stereochemical restraints in refinement, the distance from the Schiff base nitrogen (NZ) to retinal C4 increases from 14.0 to 14.6 Å, resulting in a more linear (or less bent) polyene chain in NpSRII. The relative positions of the protonated Schiff base nitrogen and the two negatively charged aspartate carboxylates of Asp^{75} and Asp^{201} are nearly unchanged. However, the electron density for the water molecule found between the Schiff base and these two carboxylates (Wat^{402}) (*9*, *32*) is very weak, suggesting that this water is either more mobile or not fully occupied in NpSRII. In contrast, waters 401, 406, and 501 are well ordered (*9*). The π bulge of helix G at residue 204 is also present as it is in BR (*9*) and HR (*10*), despite the bulkier side chain (Thr^{204}) at this position. (**B**) Stereo view of the Schiff base and the complex counterion. The guanidinium of Arg^{72} moves 1.1 Å away (10.5 versus 9.4 Å) from the Schiff base nitrogen and also reorients its Nε hydrogen. This movement becomes possible because several side chains in the region between Arg^{72} and the extracellular side (below Arg^{72} in the figure) have reduced volumes (Phe^{208} → Ile^{197}, Glu^{194} → Pro^{183}, and Glu^{204} → Asp^{192}). (**C**) Plot of distance versus residue number. The average main-chain distance between NpSRII and BR is plotted as a function of residue number (BR numbering). The largest deviations are at the shortened antiparallel β sheet in the BC loop (near residue 70) and at the COOH-terminus, which is being displaced by a detergent molecule.

the other retinal pocket residues from their altered positions, which are determined by residue interactions outside the pocket as well as by helix backbone differences between NpSRII and the transport rhodopsins (Fig. 2C). Arg^{72} is repositioned as a consequence of several factors, including movement of its helix backbone by 0.9 Å and the cavity created by changes from BR: $Phe^{208} \rightarrow Ile^{197}$, $Glu^{194} \rightarrow Pro^{183}$, and $Glu^{204} \rightarrow Asp^{192}$ (Fig. 2B). Hence the spectral tuning results from precise positioning of retinal binding pocket residues and the guanidinium of Arg^{72}, which cannot be deduced from primary structure alone but requires atomic-resolution tertiary structure information.

Wegener *et al.* (*20*) have used electron paramagnetic resonance spectroscopy to measure the accessibility and static and transient mobility of nitroxide labels placed at the positions of eight residues on the cytoplasmic side of helices F and G in NpSRII. They concluded that Lys^{157} and Ser^{158} are oriented toward the aqueous phase; Leu^{159}, Tyr^{160}, Ile^{211}, and Leu^{213} face the protein interior; and Phe^{210} and Ala^{212} are located at the protein/lipid bilayer interface. Each of these assignments is confirmed by the crystal structure except Ile^{211}, which is on the surface of helix G facing the hydrophobic portion of the bilayer. A possible explanation of the contrasting assignment of Ile^{211} is that the spin-label nitroxide distorts the structure. Further, light-induced changes in the spin labels indicated movement of helix F with negligible movement of helix G (*20*). The disconnection of the two helices was suggested as possibly being due to the predicted absence of the π bulge in helix G (*20*), but we observe the π bulge to be present in the NpSRII structure, indicating that the apparent dissociation of helixes F and G in the spin-labeling study must be attributable to other factors.

The sensory rhodopsins do not pump ions when complexed with their cognate transducers, but in some cases light-driven vectorial translocation of protons does occur in the absence of transducer (*21*). Substantial proton transport by NpSRII required factors that are expected to increase cytoplasmic-side proton conductivity (the presence of sodium azide and the $Phe^{86} \rightarrow Asp^{86}$ mutation), and both wild-type NpSRII and HsSRII circulate protons primarily to and from the extracellular side. In the structure, the low proton conductivity on the cytoplasmic side is evident in that the Asp^{96}-Thr^{46} pair in the cytoplasmic channel of BR is replaced by the Phe^{86}-Leu^{40} pair and presents a hydrophobic barrier (*22*). The greater hydrophobicity of the cytoplasmic side is attested by the presence of a detergent molecule (β-octylglucoside) that is inserted with its C8 tail perpendicular to the bilayer into the middle of the seven-helix bundle, almost reaching the side chain of Phe^{86}.

A fundamental question is how the common design of microbial rhodopsin proteins has been adapted to carry out their two distinct functions. Transport rhodopsins function independently of interaction with other proteins and translocate ions through an intramolecular channel. Sensory rhodopsins, on the other hand, transmit signals by protein-protein interaction with transducer proteins that control cytoplasmic enzymatic activity (*7*, *23*, *24*). In HsSRI and HsSRII, the receptors form a molecular complex with their cognate integral membrane transducer proteins, HtrI and HtrII, respectively, which in turn modulate a cytoplasmic phosphorylation pathway that controls the cell's motility apparatus (*1*). Chimera experiments with the *H. salinarum* transducers showed that the interaction specificities of SRI with HtrI and SRII with HtrII are determined by the transmembrane helices of the Htr subunits (*25*), indicating that interaction occurs within or near the membrane. A fragment of NpHtrII lacking most of the cytoplasmic domain interacts with NpSRII in vitro, supporting the idea that transmembrane helix-helix interactions occur also in the *N. pharaonis* pair (*20*). Bearing on the possible location of the transducer-binding surface of the receptor, the structure of NpSRII reveals that a tyrosine residue protrudes from the lipid-facing surface of helix G (Fig. 3). Unlike threonine or serine hydroxyls, which can hydrogen-bond to main-chain carbonyls of their own helix, the tyrosine phenol group is too long and rigid to allow the formation of such hydrogen bonds. To avoid an unpaired polar hydroxyl in the middle of the bilayer, in the 3D crystals, and presumably in the 2D crystals as well, the Tyr^{199} hydroxyl forms an intermolecular hydrogen bond to the main-chain carbonyl of a transmembrane helix from a neighboring molecule in the same bilayer (Ala^{125} in helix E). Tyr^{199} is conserved in the three known SRII sequences, whereas this residue is a phenylalanine in the two known SRI sequences (*1*). The need to hydrogen-bond to an adjacent protein makes Tyr^{199} an excellent candidate for transducer binding in the SRII-HtrII complex in *N. pharaonis* membranes. The hydrophobic surface of NpSRII displays three distinct faces: face I is defined by helices F, G, and A; face II by helices A (the CP half), B, C, D, and E (the EC half); and face III by helices E and F. Tyr^{199} is located prominently in the middle of face I, the face that also contains both helices known to undergo large motions during the BR photocycle (*26*). It is thus likely that face I provides the majority of the interaction with the photosignal transducer. Other residues on the outside of helix G also show clear grouping between the SRI and SRII subfamilies, possibly contributing to transducer binding specificity.

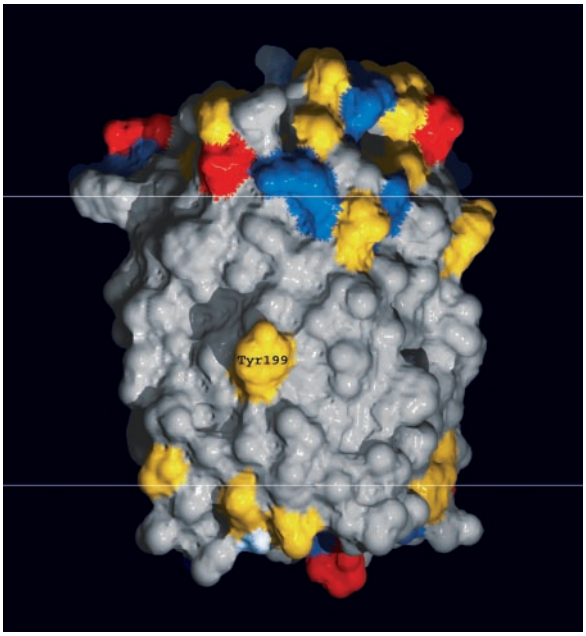

Fig. 3. Exposed conserved tyrosine in middle of the bilayer. The NpSRII surface (CP side, top; EC side, bottom) is colored according to amino acid type (red, negatively charged; blue, positively charged; yellow, polar; gray, hydrophobic). Residue Tyr^{199} is situated in the middle of the bilayer (whose hydrophobic portion lies between the white horizontal lines) near a π bulge on the outside of helix G one-and-a-half helix turns from the lysine (Lys^{205}) to which the retinal is attached.

References and Notes

1. W. D. Hoff, K.-H. Jung, J. L. Spudich, *Annu. Rev. Biophys. Biomolec. Struct.* **26**, 223 (1997).
2. D. Oesterhelt, *Curr. Opin. Struct. Biol.* **8**, 489 (1998).
3. J. K. Lanyi, *J. Phys. Chem.* **104**, 11441 (2000).
4. O. Béjà *et al.*, *Science* **289**, 1902 (2000).
5. J. A. Bieszke, E. N. Spudich, K. L. Scott, K. A. Borkovich, J. L. Spudich, *Biochemistry* **38**, 14138 (1999).
6. J. L. Spudich, C.-H. Yang, K.-H. Jung, E. N. Spudich, *Annu. Rev. Cell. Dev. Biol.* **16**, 365 (2000).
7. R. Seidel *et al.*, *Proc. Natl. Acad. Sci. U.S.A.* **92**, 3036 (1995).
8. H. Belrhali *et al.*, *Structure* **7**, 909 (1999).
9. H. Luecke, B. Schobert, H.-T. Richter, J.-P. Cartailler, J. K. Lanyi, *J. Mol. Biol.* **291**, 899 (1999).
10. M. Kolbe, H. Besir, L. O. Essen, D. Oesterhelt, *Science* **288**, 1390 (2000).
11. E. R. S. Kunji, E. N. Spudich, R. Grisshammer, R. Henderson, J. L. Spudich, *J. Mol. Biol.* **308**, 279 (2001).
12. T. Takahashi *et al.*, *Biochemistry* **29**, 8467 (1990).
13. J. Hirayama *et al.*, *Biochemistry* **31**, 2093 (1992).
14. I. Chizov *et al.*, *Biophys. J.* **75**, 999 (1998).

15. K. Nakanishi *et al.*, *Photochem. Photobiol.* **29**, 657 (1979).
16. B. Yan *et al.*, *J. Biol. Chem.* **270**, 29668 (1995).
17. J. L. Spudich *et al.*, *Biophys. J.* **49**, 479 (1986).
18. K. Shimono, M. Iwamoto, M. Sumi, N. Kamo, *Photochem. Photobiol.* **72**, 141 (2000).
19. N. Kamo, K. Shimono, M. Iwamoto, Y. Sudo, *Biochemistry* (*Moscow*), in press.
20. A. A. Wegener, I. Chizhov, M. Engelhard, H. J. Steinhoff, *J. Mol. Biol.* **301**, 881 (2000).
21. HtrI-free HsSRI was shown to exhibit single photon–induced proton pumping out of cell envelope vesicles at pH $>$ 7 [R. A. Bogomolni *et al.*, *Proc. Natl. Acad. Sci. U.S.A.* **91**, 10188 (1994)]. In cell envelope vesicles, HsSRII exhibits only electroneutral light-induced circulation of protons to and from the extracellular medium [J. Sasaki, J. L. Spudich, *Biophys. J.* **77**, 2145 (1999)]. NpSRII was found to have some proton transport activity in such vesicles [Y. Sudo, M. Iwamoto, K. Shimono, M. Sumi, N. Kamo, *Biophys. J.* **80**, 916 (2001)] as well as in black lipid films [G. Schmies *et al.*, *Biophys. J.* **78**, 959 (2000)]. When expressed in *Xenopus* oocytes, HsSRII exhibited weak proton transport and NpSRII did not show any stationary photocurrent [G. Schmies, M. Engelhard, P. G. Wood, G. Nagel, E. Bamberg, *Proc. Natl. Acad. Sci. U.S.A.* **98**, 1555 (2001)].
22. The cytoplasmic region of NpSRII lacks a nucleation site for the development of a hydrogen-bonded network of water molecules [H. Luecke *et al.*, *J. Mol. Biol.* **300**, 1237 (2000)]. Also, the extracellular region lacks proton release machinery; that is, a pair of glutamic acid residues connected to the Schiff base region by a 3D hydrogen-bonded network of side chains and water (*9*) [R. Rammelsberg, G. Huhn, M. Lübben, K. Gerwert, *Biochemistry* **37**, 5001 (1998)] that prevents the return of the proton from the extracellular side in bacteriorhodopsin [S. P. Balashov, E. S. Imasheva, R. Govindjee, T. G. Ebrey, *Biophys. J.* **70**, 473 (1996); H.-T. Richter, L. S. Brown, R. Needleman, J. K. Lanyi, *Biochemistry* **35**, 4054 (1996)]. A similar situation arises in the $Asp^{96} \rightarrow Asn^{96}$ mutant of BR at a pH below the pK for proton release; but unlike NpSRII, this protein exhibits transport. In BR, although at pH $<$ 6 protonation equilibrium between the Schiff base and its counterion ensures that the proton can pass to the extracellular side [L. S. Brown, A. K. Dioumaev, R. Needleman, J. K. Lanyi, *Biophys. J.* **75**, 1455 (1998)], at the low pH the reprotonation from the cytoplasmic side is strongly accelerated [A. Miller, D. Oesterhelt, *Biochem. Biophys. Acta* **1020**, 57 (1990)]. In contrast, the cytoplasmic region of NpSRII is likely to be a permanent barrier to protons. If directionality is conferred on the movement of the transported ion by the changing ion conductivities of the extracellular and cytoplasmic regions [L. S. Brown, A. K. Dioumaev, R. Needleman, J. K. Lanyi, *Biochemistry* **37**, 3982 (1998)], reprotonation of the Schiff base in NpSRII will be, of necessity, from the extracellular rather than the cytoplasmic side.
23. V. J. Yao, J. L. Spudich, *Proc. Natl. Acad. Sci. U.S.A.* **89**, 11915 (1992).
24. W. Zhang, A. Brooun, M. M. Mueller, M. Alam, *Proc. Natl. Acad. Sci. U.S.A.* **93**, 8230 (1996).
25. X.-N. Zhang, J. Zhu, J. L. Spudich, *Proc. Natl. Acad. Sci. U.S.A.* **96**, 19722 (1999).
26. S. Subramaniam, R. Henderson, *Nature* **406**, 653 (2000).
27. E. M. Landau, J. P. Rosenbusch, *Proc. Natl. Acad. Sci. U.S.A.* **93**, 14532 (1996).
28. Z. Otwinowski, in *Data Collection and Processing*, L. Sawyer, N. Isaacs, S. Bailey, Eds. (SERC Daresbury Laboratory, Warrington, UK, 1993), pp. 56–62.
29. A. T. Brunger, *X-PLOR, Version 3.1: A System for X-Ray Crystallography and NMR* (Yale Univ. Press, New Haven, CT, 1992).
30. A. T. Brunger *et al.*, *Acta Crystallogr. D* **54**, 905 (1998).
31. J. S. Sack, *J. Mol. Graphics* **6**, 224 (1988).
32. H. Luecke, H. T. Richter, J. K. Lanyi, *Science* **280**, 1934 (1998).
33. N. Guex, M. C. Peitsch, *Electrophoresis* **18**, 2714 (1997).
34. We thank R. R. Birge for discussions regarding spectral tuning in NpSRII and BR, C. Riekel for access to the microfocus beamline at the European Synchrotron Radiation Facility (ESRF), and J.-P. Cartailler for assistance with Fig. 2C. Supported by NIH grants R01-GM59970 (H.L.), R01-GM29498 (J.K.L.), and R01-GM27750 (J.L.S.); Department of Energy grant DEFG03-86ER13525 (J.K.L.); and a Robert A. Welch Foundation award (J.L.S.). The atomic coordinates of NpSRII have been deposited in the Protein Data Bank (PDB) with the entry name of 1JGJ.

30 May 2001; accepted 27 June 2001
Published online 12 July 2001;
10.1126/science.1062977
Include this information when citing this paper.

Selective Transcription and Modulation of Resting T Cell Activity by Preintegrated HIV DNA

Yuntao Wu and Jon W. Marsh*

The quiescent nature of most peripheral T cells poses an effective limitation to human immunodeficiency virus (HIV) replication and, in particular, to viral integration into the host chromatin. Two HIV proteins, Nef and Tat, increase T cell activity, but a requirement of integration for viral gene expression would preclude a role for these proteins in resting cells. Here, we report that HIV infection leads to selective transcription of the *nef* and *tat* genes before integration. This preintegration transcription in quiescent cells leads to increased T cell activation and viral replication.

Replication of HIV predominates in the CD4 T cell population (*1*), and the level of replication is highly prognostic for the development of acquired immunodeficiency syndrome (AIDS) (*2*). However, viral infection is limited by the quiescence of most circulating T cells, which is nonsupportive of viral replication. As a retrovirus, the RNA genome of HIV undergoes reverse transcription to a DNA intermediate, followed by integration into the host chromatin. Formation of the integrated provirus is essential for HIV replication (*3*–*5*), and yet the most prevalent form of HIV DNA during the asymptomatic phase of infection is full-length unintegrated DNA (*6*). The barrier to integration seen in peripheral T cells can be overcome by stimulatory increases in the cellular metabolic state through either mitogenic (*3*, *7*, *8*) or submitogenic (*9*, *10*) stimulation. Recent findings suggest that HIV may have evolved functions to overcome this threshold. Expression of the earliest HIV gene products, Nef and Tat, can increase T cell activity (*11*–*15*), and in particular, Nef can lower the activation threshold in T cells (*14*). However, it is unclear how these HIV proteins could promote the early and limiting steps of infection (and integration) if provirus formation is required first.

To define the capacity of HIV to affect the activation state of quiescent primary CD4 T cells, we explored the earliest events in HIV infection. Quiescent CD4 T cells were infected with the NL4-3 strain of HIV-1 at 0.5 infectious virions per cell. After 5 days of incubation, during which no measurable viral replication occurred (*16*), cells were stimulated through their T cell receptors with CD3 plus CD28 (CD3-CD28) immobilized antibody beads and were measured for interleukin-2 (IL-2) (Fig. 1). IL-2 is the definitive indicator of CD4 T cell activation, a condition optimal for viral integration and replication. The expression of IL-2 is mediated by transcription factors also responsible for the HIV long terminal repeat (LTR) promoter activity (*17*). We observed a stimulus-dependent increase in IL-2 generation in resting cells exposed to HIV (Fig. 1).

The binding of the HIV envelope to cellular receptors (*18*, *19*) or the inclusion of Nef in the virion (*20*) could alter the activation state of the T cell before integration. To distinguish between activation through these existing virion components or newly synthesized viral products, we incubated purified resting CD4 T cells with HIV in the presence or absence of the reverse transcriptase inhibitor 3′-azido-3′-deoxythymidine (AZT). The addition of AZT to the T cells did not affect the level of IL-2 generated by CD3-CD28 bead activation (*21*). However, the HIV-enhanced IL-2 response was lost in the presence of AZT (Fig. 1, donors 3 and 4). This implies that the reverse transcription and its downstream products, and not virion-cellular interactions, were responsible for the enhancement of T cell activation.

We then examined the state of the HIV DNA and the transcriptional activity of the DNA in quiescent cells. Resting T cells were

Laboratory of Molecular Biology, National Institute of Mental Health, Bethesda, MD 20892–4034, USA.

*To whom correspondence should be addressed. E-mail: jon@codon.nih.gov